Title

Investigation of long term drift of an intraocular pressure sensor

Journal

Microsystem Technologies, 27(6)

ISSN

1099-8047

Authors

Phan, Alex
Truong, Phuong
Schade, Christoph
et al.

Publication Date

2021-06-01

DOI

10.1007/s00542-020-05164-2

Peer reviewed

ANALYTICAL MODELING OF AN IMPLANTABLE OPTO-MECHANICAL PRESSURE SENSOR TO STUDY LONG TERM DRIFT

Alex Phan, Phuong Truong, Christoph Schade, Aditya Vasan, James Friend and Frank E. Talke
University of California, San Diego, La Jolla, CA
Center for Memory and Recording Research

ABSTRACT

"Zero drift" behavior of an optical intraocular pressure sensor is studied using an analytical model based on the deflection of a circular membrane. Results from the analytical model were verified with experimental results from "bulge" testing. The analytical model was used to study the "zero drift" of the sensor as a function of changes in membrane thickness, geometry of the sensor and amount of gas inside the cavity of the sensor. The results show that dissolution of the membrane, swelling of the spacer layer and oxidative aging can contribute significantly to zero drift of the sensor over time. The results are useful in guiding design and fabrication optimization to minimize drift in intraocular pressure sensors used for long term implantation.

Keywords: implantable pressure sensor, MEMS, zero drift, silicon nitride dissolution, hygroscopic swelling, oxidative aging

1. INTRODUCTION

In this paper, we investigate the "zero drift" behavior of an optical intraocular pressure sensor due to membrane dissolution, hygroscopic swelling, and oxidative aging of the epoxy spacer layer. The opto-mechanical pressure sensor is an 800 µm diameter MEMS device consisting of a deflecting silicon nitride (SiN) membrane, an SU-8/epoxy layer as a spacer, and a glass substrate (Fig. 1). Deflection of the membrane is a function of the intraocular pressure. When the sensor is exposed to monochromatic light, the reflected light waves at the bottom and the top of the cavity of the sensor interfere with each other and form optical interference fringes. These fringe patterns can be captured using a handheld reader and the images can then be processed to determine the intraocular pressure. Fig. 2 shows typical interference fringe patterns obtained at various pressures from 0 to 60 mmHg.

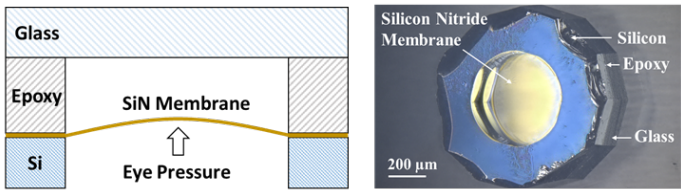

Figure 1: Schematic of the opto-mechanical intraocular pressure sensor (left) and photograph of a fabricated sensor (right).

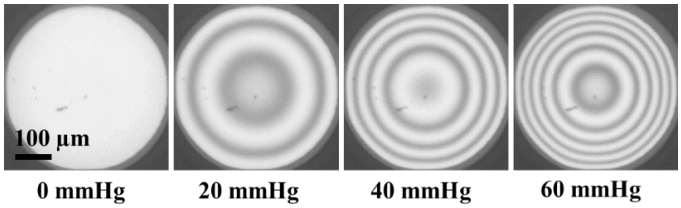

Figure 2: Typical interference fringes patterns formed at the cavity of the sensor at various pressure loads from 0-60 mmHg.

In a prior *in vivo* study [1], we have successfully implanted an interferometric pressure sensor in a New Zealand White rabbit and obtained direct measurements of the intraocular pressure of one of the rabbit's eyes. However, a drift in the sensor's pressure reading was observed over the next several months (Fig. 3).

Drift of a pressure sensor is undesirable since it can lead to substantial error if uncorrected. It is especially undesirable in this application, as it could lead to errors in diagnosing glaucoma. Potential sources of drift include the dissolution (thinning) of the silicon nitride membrane, the swelling of the epoxy spacer layer, and changes in the amount of gas inside the cavity of the sensor. The goal of this study is to isolate the effect of membrane thinning, epoxy swelling, and oxidative aging, respectively, in order to characterize their individual contributions to zero drift of the sensor as a function of time. The results from the study can be used to guide the design and fabrication process in the development of the sensor and minimize its zero drift behavior.

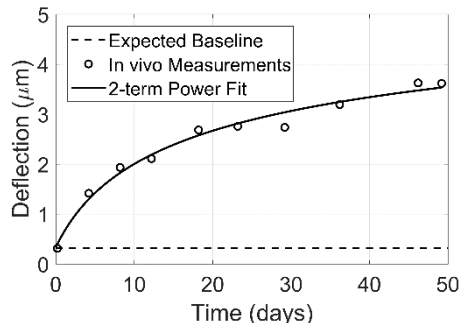

Figure 3: Zero drift observed during *in vivo* study (New Zealand White rabbit). The measured membrane deflection increased over time despite minimal fluctuations in eye pressure.

2. MATERIALS AND METHODS

2.1 Theory

A schematic of the intraocular pressure sensor is shown in Fig. 4. The sensor consists of a silicon nitride membrane, a spacer layer, and a glass substrate. The cavity of the sensor (radius R_c and height h) is sealed during fabrication at atmospheric pressure and room temperature. As the membrane deflects inward due to the intraocular pressure P_{ex}, the gas inside the cavity of the sensor is compressed resulting in an elevated pressure P_{in} acting on the inner surface of the membrane of the sensor.

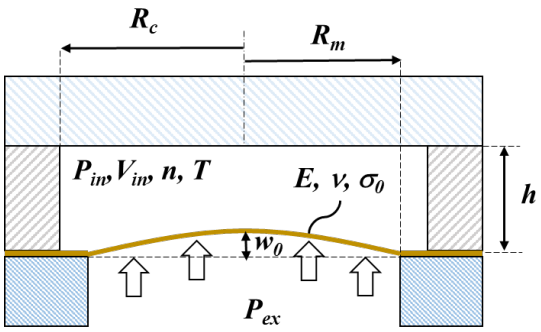

Figure 4: Schematic of the interferometric intraocular pressure sensor

The relationship between the external pressure P_{ex} and the maximum deflection w_o at the center of the circular membrane of radius R_m is given by [2]

$$P_{ex} = 4\left(\frac{\sigma_0 t}{R_m^2}\right) w_0 + \left(\frac{8}{3}\frac{Et}{R_m^4(1-\upsilon)}\right) w_0^3 + P_{in} \qquad (1)$$

where σ_o is the residual stress in the membrane and R_m, t, E, and ν are the radius, the membrane thickness, the Young's modulus and the Poisson's ratio of the membrane, respectively. The first term in Eq. 1 describes the contribution from the residual stress of the membrane and the second term describes the contribution from the deformation of the membrane. Contribution from bending stiffness is neglected since we are considering large deflections of a thin membrane ($w_0 \gg t$).

The internal pressure can be determined using the ideal gas law:

$$P_{in} = \frac{nRT}{V_{in}} \qquad (2)$$

where V_{in} is the internal volume of the cavity, n is the number of moles of gas in the cavity, R is the gas constant and T is the temperature. For an undeflected membrane, the internal volume of the cavity is $V_{in} = V_0 = \pi R_c^2 h$. The deflection of the circular membrane as a function of the radius R_m may be approximated by

$$w(r) = w_o\left(1 - \frac{r^2}{R_m^2}\right) \qquad (3)$$

Combining Eqns. (1)-(3), we obtain the following fourth order equation for the maximum membrane deflection w_o as a function of the sensor design parameters and the external pressure P_{ex}

$$\left(\frac{4}{3}\frac{Et}{R_m^2(1-\upsilon)}\right)\pi w_o^4 - \left(\frac{8}{3}\frac{Et}{R_m^4(1-\upsilon)}\right)V_0\, w_0^3 + 2\sigma_0 t\pi w_o^2 - \left(\frac{\pi R_m^2}{2}P_{out} + 4\left(\frac{\sigma_0 t}{R_m^2}\right)V_o\right)w_o + P_{out} * V_o - nRT = 0 \qquad (4)$$

2.2 Material Properties and Sensor Characterization

In order to use Eq. (4) for the design of a sensor, material properties of the sensor such as the Young's modulus E and the residual stress σ_o of the membrane are needed. These values were obtained from material testing.

To obtain the Young's modulus and the residual stress of the membrane, a so-called "bulge" test was performed, deflecting the membrane under pressure and measuring the deflection [3]. In the present study, a 500 µm wide and 200 nm thick circular SiN membrane was mounted on a 5 mm x 5 mm silicon support frame and placed in a custom-made test chamber. Pressure from 0 mmHg to 100 mmHg in steps of 1 mmHg was applied onto the membrane, resulting in a pressure versus maximum deflection curve. To determine E and σ_o from Eq. 1 we divided both sides by $4\sigma_0 t/R_m^2$, producing

$$P\left(\frac{R_m^2}{4tw_0}\right) = \sigma_0 + \frac{2}{3}\frac{E}{(1-\upsilon)}\frac{w_0^2}{R_m^2} \qquad (5)$$

Plotting the experimental data from the bulge test as $P = P(w_0)$ and shown in Eq. 5, one can obtain the residual stress (σ_o = 110 MPa) and the Young's modulus (E = 210 GPa) from the intercept and the slope of the linear curve fit for Eq. 5, respectively (Fig. 5).

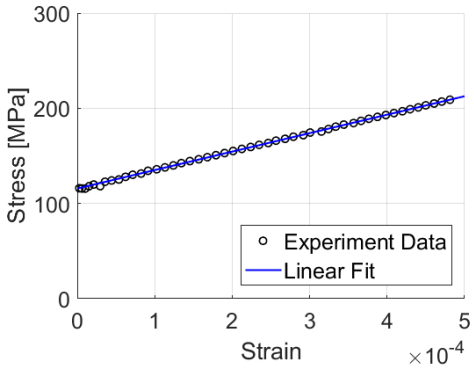

Figure 5: Bulge test results for a circular silicon nitride membrane: residual stress, σ_o, and Young's modulus, E, can be extracted from the intercept and slope values of the fitted linear curve.

From Fig. 5 we observe that the residual stress of the SiN membrane is σ_o = 110 MPa. This value was significantly different from the residual stress value of 250 MPa reported by the manufacturer at the wafer level (Norcada Inc.). To further investigate this discrepancy, we employed a second method to measure the residual stress in the SiN thin film using resonant frequency and displacement measurements.

The SiN membrane was first mounted on a lithium niobate piezoelectric substrate. The piezoelectric substrate was then excited with an input frequency from 50 Hz to 1.5 MHz using a function generator (Agilent Technologies). This induced mechanical vibration of the membrane. A Polytec UHF-120SV scanning laser Doppler vibrometer (Polytec GmbH) was used to capture the vibration profiles of the membrane at various resonance frequencies (Fig. 6). The resonance frequencies are functions of the residual stress of the membrane. The residual stress was determined to be $\sigma_o = 98 \pm 7$ MPa. This result agrees well with the value of $\sigma_o = 110 \pm 10$ MPa obtained from the bulge test experiment.

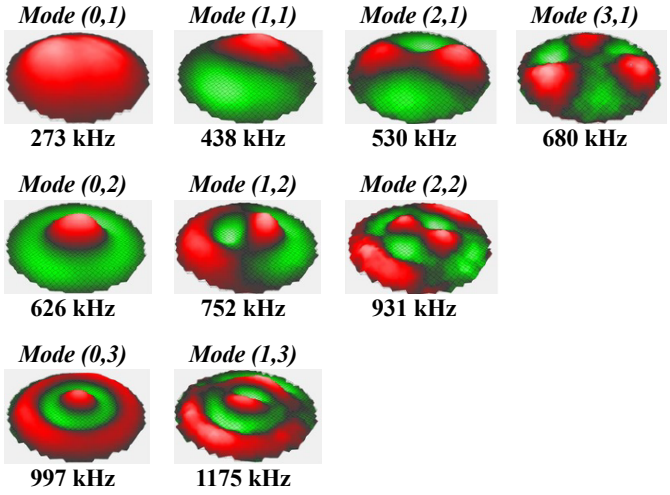

Figure 6: Mode shapes of the circular SiN membrane captured at various resonance frequency using a scanning laser Doppler vibrometer.

In Fig. 6, typical resonance shapes of the membrane are shown. Distinct nodal circles and nodal diameters can be seen. The dimensions of the sensor were also obtained for the analytical model. The thickness of the membrane t was measured to be 200 nm (Filmetrics F20). This is consistent with the reported value from the manufacture (Norcada Inc.). An AFM scan (Digital Instruments, Dimension 3000) was performed on a cross section of the sensor to determine the thickness of the epoxy spacer layer. The height of the cavity h was measured to be 10.8 µm as shown in Fig. 7.

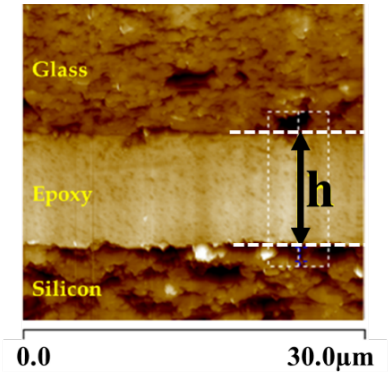

Figure 7: An AFM scan of a cross section of the fabricated sensor.

Finally, with the analytical model derived and material properties and sensor dimensions determined, the drift behavior was studied as a function of the change in membrane thickness, spacer layer height and amount of gas inside the cavity of the sensor. A change in membrane thickness t can be caused by dissolution (thinning) of the SiN membrane. A change in the spacer layer height h can be caused by hygroscopic swelling of the epoxy. A change in the amount of gas inside the sensor cavity n can be caused by oxidative aging of the epoxy layer.

3. RESULTS AND DISCUSSION

3.1 Analytical Model Validation

The analytical model (Eq. 4) was first verified against experimental data to validate the results from the model. The parameters of a typical sensor are listed in Table 1.

Parameter	Symbol	Value	Unit
Thickness of membrane	t	200	nm
Radius of membrane	R_m	250	µm
Young's modulus	E	210	GPa
Poisson's ratio	υ	0.27	
Residual stress	σ_o	110	MPa
Radius of cavity	R_c	300	µm
Height of cavity	t	10.8	µm
Gas inside cavity	n	1.27^{-10}	moles

Table 1: Parameters of a typical IOP sensor

Using a pressure regulator setup [1], we applied pressure from 0 to 100 mmHg to the sensor and captured the interference pattern. Image processing was then performed to determine the maximum value of the deflection of the membrane at each pressure. As shown in Fig. 8, the analytical and experimental calibration results correlated well with the root mean square (RMS) error of less than ±0.02µm.

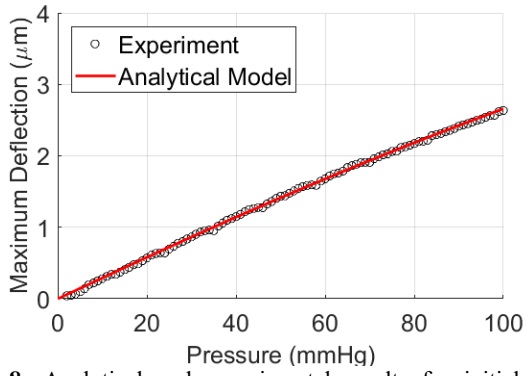

Figure 8: Analytical and experimental results for initial sensor calibration curve in the range from 0 mmHg to 100 mmHg.

3.2 Parameter Contribution to Sensor Behavior

In order to investigate how the thickness of the membrane, the height of the cavity of the sensor, and the amount of gas inside the cavity of the sensor contribute to the drift behavior, we first studied their individual contributions to the response of the sensor. We isolated each effect and showed how changes in the thickness of the membrane (Fig. 9), in the height of the cavity (Fig. 10), and in the amount of gas inside the cavity (Fig. 11) can contribute to the shift of the initial calibration curve of the sensor.

In Fig. 9, the calibration curve of the sensor is shown for three values of the membrane thickness (200 nm, 150 nm, 100nm). We observe that maximum deflection increases with decreasing membrane thickness. The average sensitivity of the sensor can be calculated by taking the ratio of the maximum deflection range and the pressure range. The results show that the sensitivity of the sensor increases by 10%, from 30 nm/mmHg to 35 nm/mmHg, as the membrane thickness decreases by 50%, from 200 nm to 100 nm.

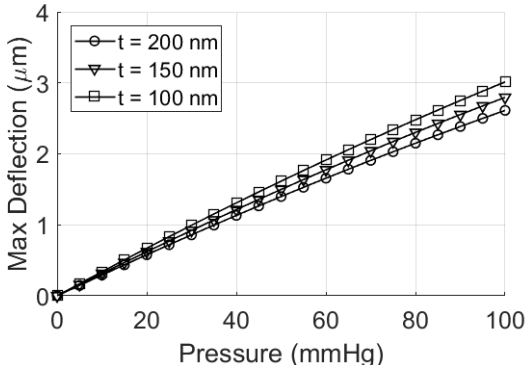

Figure 9: Calibration curves of the sensor as a function of membrane thickness, *t*. The height of the cavity, *h*, was fixed at 10 µm and the amount of gas inside the cavity, *n*, was fixed at 1.27^{-10} moles.

In Fig. 10, we have varied the height of the cavity from 10 µm to 10.2 µm and fixed all other parameters. We observe that the calibration curve of the sensor shifts upward with increasing cavity height. The difference in the sensitivity of the sensor in these three cases are relatively small, less than 1%. However, the vertical shift in the calibration curve leads to a 20-mmHg difference in pressure for the same maximum deflection value when the height of the cavity increases by 2%, from 10 µm to 10.2 µm.

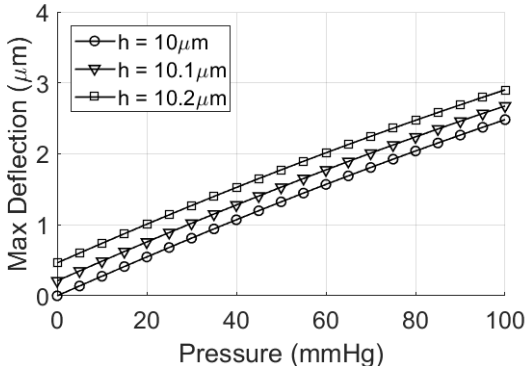

Figure 10: Calibration curves of the sensor as a function of cavity height, *h*. The thickness of the membrane, *t,* was fixed at 200 nm and the amount of gas inside the cavity, *n*, was fixed at 1.27^{-10} moles.

Fig. 11 shows the effect of changes in the number of moles of gas inside the cavity of the sensor. As the amount of gas decreases from the initial value of 1.27^{-10} moles to 1.22^{-10} moles, the calibration curve of the sensor shifts upward. Changes in the sensitivity of the sensor are relatively small, less than 1%, and similar to the previous case considering a change in the cavity height. The results show that for the same external pressure, a 2% decrease in the quantity of gas inside the cavity of the sensor leads to a 0.6 µm difference in the maximum deflection value.

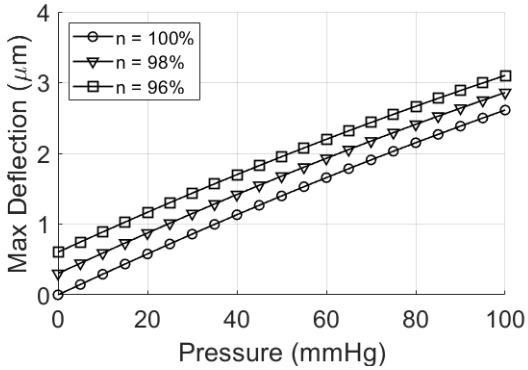

Figure 11: Calibration curves of the sensor as a function of amount of gas inside the cavity of the sensor, *n,* where 100% corresponds to 1.27^{-10} moles. The height of the cavity, *h*, was fixed at 10 µm and the thickness of the membrane, *t,* was fixed at 200 nm.

We observe that the maximum deflection of the membrane is a function of the external pressure, the membrane thickness, the cavity height, and the number of moles of gas inside the cavity. Clearly, these parameters must be considered as contributing factors as we investigate methods to reduce the drift behavior of the intraocular pressure sensor.

3.3 Contributions of SiN Dissolution, Epoxy Swelling and Oxidative Aging to Drift Behavior

In the following section, we study the effect of SiN dissolution, epoxy swelling and oxidative aging of the epoxy layer on the response of the sensor.

Remarkably, silicon nitride does dissolve while exposed to phosphate buffered saline. A typical silicon nitride membrane dissolution rate of 0.33 nm/day was obtained from silicon nitride dissolution experiments using phosphate buffered saline solution at 37°C [4]. Thus, assuming the membrane thickness decreases from 200 nm to 80 nm in one year, the characteristic of the sensor changes as shown in Fig. 9. This causes an increase in the pressure readout that is higher than that corresponding to the constant applied pressure. In the case under investigation, the dissolution of the SiN membrane at 0.33 nm/day results in a 3-mmHg drift in the first year (Fig. 12). It is worth noting that as the dissolution process continues, the thickness of the membrane will approach zero in just under two years at the given dissolution rate. This will lead to failure of the sensor.

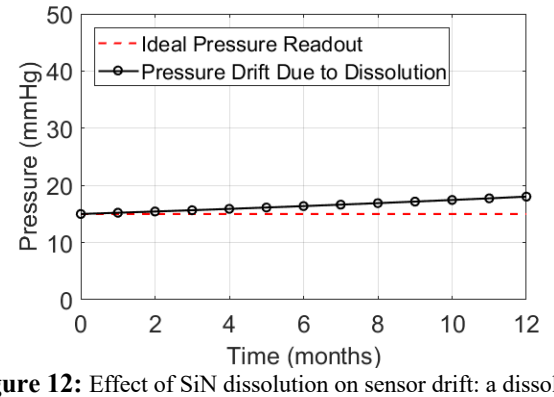

Figure 12: Effect of SiN dissolution on sensor drift: a dissolution rate of 0.33nm/day leads to a 3-mmHg drift over one year.

Next, the time-dependent change in the height of the spacer layer was obtained from epoxy swelling experiments in which a 10 μm layer of epoxy was submerged in saline solution under 15 mmHg of pressure. Since the epoxy layer of the sensor absorbs water and swells over time, the height of the layer increases. This leads to an increase in the volume of the cavity and a decrease in the internal pressure. In the present study, a 2% increase in the height of the cavity leads to a 17-mmHg drift in the pressure readout over the course of one year as shown in Fig. 13.

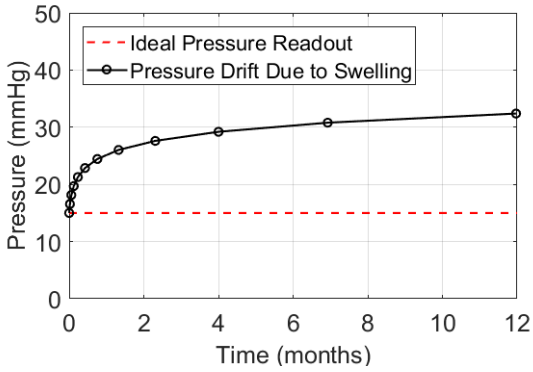

Figure 13: Effect of hygroscopic swelling of the epoxy layer on sensor drift: a 2% increase in the epoxy layer leads to a 17-mmHg drift over one year.

Finally, changes in the amount of gas (number of moles) inside the cavity of the sensor can cause an "upward" or "downward" zero drift. Outgassing from the SU-8 and epoxy layer into the cavity within increases the amount of gas in the cavity of the sensor and leads to a "downward" zero drift [5]. On the other hand, oxidative aging (oxidation reaction) reduces the amount of oxygen molecules present in the cavity and leads to an "upward" zero drift [6]. The effect of oxidative aging was found to be very significant in the present case: a change of more than 33 mmHg over the course of six months as the amount of oxygen in the cavity of the sensor decreases by half [7], i.e., 10% of the total amount of gas inside the cavity (Fig. 14).

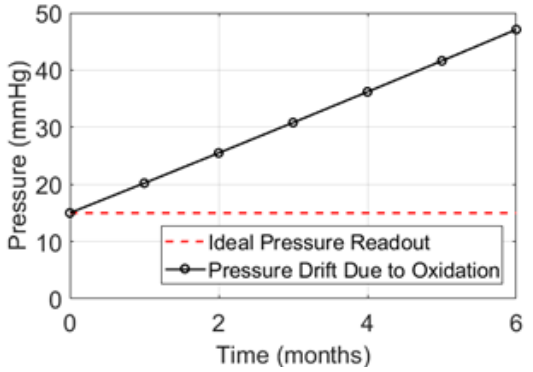

Figure 14: Effect of oxidative aging of the epoxy layer on sensor drift: a 50% drop in the amount of oxygen leads to a 33-mmHg drift over six months.

The results of the analytical model show that SiN membrane dissolution, hygroscopic swelling, and oxidative aging of the epoxy spacer layer can contribute to an "upward" zero drift of the sensor where the measured pressure is higher than the actual pressure. These effects can cause a long-term drift of the sensor that can be characterized by the dissolution rate of SiN, the diffusion rate of water into the epoxy layer, and the oxidative aging rate of the epoxy layer.

In order to improve the long-term drift performance of the sensor, it is important to minimize the effects of these phenomena. For instance, an additional protective layer, such as

titanium oxide or parylene C, can be coated around the sensor to minimize interactions between the aqueous humor and the components of the sensor, thereby improving the long-term stability of the SiN membrane and the sensor. In addition, epoxy with minimal hygroscopic expansion should be used to fabricate the sensor. Lastly, the internal cavity of the sensor can be filled with inert gas such as nitrogen, argon, or sulfur hexafluoride to prevent oxidation reaction of the epoxy layer.

4. CONCLUSION

Results from this study provide an improved understanding of the drift behavior of an intraocular pressure sensor after implantation. We provide an analytical model that considers pressure as a function of maximum deflection. We isolate parameters such as membrane thickness, cavity height, and moles of gas to observe their effects on the maximum membrane deflection. The results provide a base for the understanding the contributions of physical changes such as membrane thinning, hygroscopic swelling, and oxidative aging, that may ultimately result in zero drift behavior. The analytical work provides a direction for sensor optimization during the fabrication process to minimize drift behavior.

REFERENCES

[1] Phan et al. *IEEE Transactions on Biomed. Eng.*, 2019
[2] Senturia, S. D. *Springer US,* 2001
[3] Mitchell, J. S. *Journal of Aerospace Eng.*, 2003
[4] Schade et al. ISPS 2020
[5] Melai, J. Microelectronix Systems, 2009
[6] Celine, M. Polymer, 2013
[7] Oxidative aging of polymer